Extracellular Assembly of the Elastin Cable Line Element in the Developing Lung

CRISTIAN D. VALENZUELA,[1] WILLI L. WAGNER,[2] ROBERT D. BENNETT,[1] ALEXANDRA B. YSASI,[1] JANEIL M. BELLE,[1] KARIN MOLTER,[3] BEATE K. STRAUB,[3] DONG WANG,[4] ZI CHEN,[4] MAXIMILIAN ACKERMANN,[2] AKIRA TSUDA,[5] AND STEVEN J. MENTZER[1]*

[1]Laboratory of Adaptive and Regenerative Biology, Brigham & Women's Hospital, Harvard Medical School, Boston, MA

[2]Institute of Functional and Clinical Anatomy, University Medical Center of the Johannes Gutenberg-University, Mainz, Germany

[3]Institute of Pathology, University Medical Center of the Johannes Gutenberg-University, Mainz, Germany

[4]Thayer School of Engineering, Dartmouth College, Hanover, NH

[5]Molecular and Integrative Physiological Sciences, Harvard School of Public Health, Boston, MA

ABSTRACT

In the normal lung, a dominant structural element is an elastic "line element" that originates in the central bronchi and inserts into the distal airspaces. Despite its structural importance, the process that leads to development of the cable line element is unknown. To investigate the morphologic events contributing to its development, we used optical clearing methods to examine the postnatal rat lung. An unexpected finding was numerous spheres, with a median diameter of 1–2 μm, within the primary septa of the rat lung. The spheres demonstrated green autofluorescence, selective fluorescent eosin staining, reactivity with carboxyfluorescein succinimidyl ester, and specific labeling with anti-tropoelastin monoclonal antibody—findings consistent with tropoelastin. The sphere number peaked on rat postnatal day 4 (P4) and were rare by P14. The disappearance of the spheres was coincident with the development of the cable line element in the rat lung. Transmission electron microscopy demonstrated no consistent association between parenchymal cells and sphere alignment. In contrast, the alignment of tropoelastin spheres appeared to be the direct result of interactions of scaffold proteins including collagen fibers and fibrillin microfibrils. We conclude that the spatial organization of the cable line element appears to be independent of tropoelastin deposition, but dependent on crosslinking to scaffold proteins within the primary septa. Anat Rec, 00:000–000, 2017. © 2017 Wiley Periodicals, Inc.

Key words: alveolarization; lung development; line element; tropoelastin; murine

Abbreviations: CDF = cumulative distribution function; CFSE = carboyxfluoresein succinimydl ester; H&E = hematoxylin and eosin; PBS = phosphate buffered saline; PCLS = precision-cut lung slices; Px = postnatal day x; SEM = scanning electron microscopy; TEM = transmission electron microscopy

Grant sponsors: NIH; Grant numbers: HL134229, HL094567, CA009535, ES000002; Grant Sponsor: Branco Weiss Fellowship, ETH Zurich.

*Correspondence to Steven J. Mentzer, Room 259, Brigham & Women's Hospital, 75 Francis Street, Boston, MA 02115. Tel.: 617-732-6703; Fax: 617-730-6703 E-mail: smentzer@bwh.harvard.edu

This article was presented as an abstract at the American College of Surgeons Clinical Congress in October 2016.

Received 3 August 2016; Revised 19 December 2016; Accepted 27 December 2016.

DOI 10.1002/ar.23603

Published online 00 Month 2017 in Wiley Online Library (wileyonlinelibrary.com).

Analogous to a parachute, the structure of the peripheral lung is maintained by tensions on its cables and membranes (Butler et al., 1996). In the normal lung, the dominant cable is an elastic "line element" that originates in the central bronchi and inserts into the distal airspaces (Wagner et al., 2015). During its course, the line element forms an "ingenious" fiber continuum that supports the capillary-dense septa of alveolar walls (Weibel, 2012). The cable line element maintains septal length by balancing the effect of surface forces within the alveolus (Wilson and Bachofen, 1982); the cable line element also maintains alveolar surface area during exercise-associated changes in lung volume (Weibel, 1986). In adults, disruption of the cable leads to the impairment of both ventilation and gas exchange common to diseases such as emphysema (Azcuy et al., 1962). Congenital defects in the cable line element lead to the profound lung dysfunction associated with bronchopulmonary dysplasia (Hadchouel et al., 2014).

There are few mechanical or morphologic clues to the development of the elastin cable. The importance of mechanical stretch in normal lung development has been suggested by several clinical observations. Too little stretch—associated with oligohydramnios (Haidar et al., 1991), congenital diaphragmatic hernia (Thurlbeck et al., 1979) and phrenic nerve dysfunction (Harding et al., 1993)—has been linked to poorly developed alveolar septa and impaired gas exchange. Too much stretch, typically associated with neonatal mechanical ventilation, has been associated with disordered elastin within the alveolar walls (Pierce et al., 1997).

Morphologic clues to cable development have been largely limited to light microscopy and transmission electron microscopy (TEM). In adults, the cable line element is found at the tip of alveolar septa (Wagner et al., 2015). In classic developmental studies, Dubreuil et al. used histologic stains (fuchsine) to suggest that elastin cables were linked to the development of secondary septa (Dubreuil et al., 1936). More recently, the importance of the elastin cable was supported by the observation that alveolarization failed to occur in PDGF-A-deficient mice (Lindahl et al., 1997). In addition to failed alveolarization, elastin deficient mice demonstrated abnormal airway development (Wendel et al., 2000); elastin null mice do not survive until the alveolar stage of development. As noted by Schittny and Burri (Schittny and Burri, 2008), these studies have not addressed whether elastin producing cells are only required for the production of elastin, or whether they exert a spatial influence on cable formation.

In this report, we used a variety of morphologic techniques to illuminate the process of cable line element formation in postnatal rats; specifically, our study shows how concentrated elastin is spatially localized and aligned during the alveolarization stage of lung development.

MATERIALS AND METHODS

Animals

Outbred Wistar rats (Crl:WI) obtained from Charles River Laboratories (Wilmington, MA) were used in all experiments. A minimum of 6 animals per time point were examined on embryonic day 19, postnatal days 2, 4, 7, 14, and 21 days; 6 litters were studied to minimize litter-size effects on growth. Because of gender-independent lung growth prior to 21 days (Burri et al., 1974), no gender distinction was made in postnatal experiments. Gender-specific influences could influence subsequent growth and should be addressed in future studies (Carey et al., 2007). All 6 adult rats were females (weight range 273–435 g; age range 8–20 weeks). The experimental protocol was approved by the Institutional Animal Care and Use Committee of Harvard Medical School and Brigham and Women's Hospital.

Histology

Tissue sections were stained with a modification of a previous method (Sweat et al., 1964). Briefly, the lung tissue was prepared in thin sections and stained with commercially available hematoxylin and eosin (H&E), Sirius red, or azure blue stains. The stained tissue sections were examined using standard, fluorescent, and polarized light illumination (Puchtler et al., 1973).

Precision-Cut Lung Slices (PCLS)

To provide a supportive embedding medium for sectioning, alginic acid sodium salt (Sigma-Aldrich, St. Louis, MO) and 5% gelatin type-B (Sigma-Aldrich) in dH_2O was infused into the trachea through a 20 g Angiocath (BD Insyte, Sandy, UT), using the lowest pressure required to inflate the peripheral lung (typically 20 cm H_2O pressure). To harden the alginate, 34 mM calcium chloride and 103 mM sodium chloride in dH_2O was injected into the pulmonary artery. At total lung capacity, the trachea was clamped and the lung block was allowed to harden. Sectioning was performed with the Leica VT1000 S vibrating blade microtome (Leica Biosystems, Nussloch, Germany) using stainless steel razor blades (Gillette, Boston, MA). After sectioning, the alginate-gelatin medium was reversed by incubating the lung slices in 50 mM ethylene diamine tetraacetic acid aqueous solution (pH 7.2) at 37°C for 2 h.

Sca*l*e

PCLS fixed in glutaraldehyde were submerged in tissue-clearing medium as previously described (Hama et al., 2011). The tissue slices were incubated for 48 h at 4°C, then mounted in colorless mounting medium (Depex, VWR, Radnor, PA). The tissue was imaged using a Nikon Eclipse TE2000 inverted epifluorescence microscope using Nikon objectives with infinity correction. An X-Cite 120 watt metal halide light source (Exfo, Vanier, QC, Canada) was used to illuminate the Sca*l*e-treated samples using autofluorescence (480 nm/40 ex; 535 nm/50 em). (Chroma, Rockingham, VT). 16-bit fluorescent image stacks were digitally recorded on a C9100-02 EM-CCD camera (Hamamatsu, Japan) using MetaMorph software 7.8 (Molecular Devices, Downingtown, PA).

Decellularization

The murine lungs were decellularized using a modification of a previously described 24 hr treatment protocol (Jensen et al., 2012). Briefly, the lungs were flushed *in situ* with distilled water (dH_2O) The cardiopulmonary organs were harvested *en bloc* and submerged in dH_2O for 1 h at 4°C. The lungs were exposed to 3 sequential treatments: (1) a flush with 0.1% Triton X-100 (Sigma-Aldrich) in dH_2O and incubation for 24 h at 4°C; (2) a flush with 2% sodium deoxycholate (Sigma-Aldrich) in

dH_2O and incubated for 24 h at 4°C; and (3) a flush with 1 M sodium chloride solution and incubation for 1 h at room temperature. Finally, the lungs were treated with a 30 ug/mL bovine pancreatic DNAse (Sigma-Aldrich) solution for 1 hr at 27°C. Specimens were stored in phosphate buffered saline (Quality Biological, Gaithersburg, MD) with 5% Penicillin-Streptomycin (Life Technologies, Carlsbad, CA) at 4°C until further use.

Carboxyfluorescein Succinimidyl Ester (CFSE) Staining

The amine-reactive fluorescent probe CFSE was used to label tropoelastin as previously described (Mithieux et al., 2004). The 500 um thick lung slices were agitated in a solution of 0.5 mM CFSE (Life Technologies) in 0.1 M sodium bicarbonate buffer for 1 hr at 37°C. The lung slices were washed twice in 0.1 M sodium bicarbonate and mounted in colorless media (Depex, VWR) prior to imaging.

Anti-Tropoelastin Immunohistochemistry

Cryostat sections (20 μm thick) of postnatal lungs were warmed and blocked with 10% goat serum in PBS. The slides were treated with anti-tropoelastin antibody (ab21600, Abcam, Cambridge, MA). The slides were washed twice and treated with secondary Texas-Red-conjugated goat anti-rabbit antibody (T2767, Life Technologies, Carlsbad, CA). After 15-min incubation, the slides were washed twice, mounted in Vectashield (Vector Laboratories, Burlingame, CA) and imaged for analysis.

Electokinetic Staining

Eosin was used for to stain elastin (Heo and Song, 2011) using an electrochemical method. Briefly, a decellularized PCLS sample was embedded in a cylindrical 1% agarose gel sample layer sandwiched between a 3 mm 0.4% eosin layer (1% agarose) and a 1% agarose running layer. The sample was run for 14–16 hr at 20 mA current with a standard running buffer (250 mM glycine, 40 mM sodium chloride, 25 mM tris base, 10 mM boric acid in dH_2O and pH 7.2–7.4). The PCLS sample was removed, fixed for 20 min in 4% paraformaldehyde, washed twice in PBS, and mounted for imaging.

Scanning Electron Microscopy

After coating with 20–25 Å gold in argon atmosphere, the lung samples were imaged using a Philips XL30 ESEM scanning electron microscope (Philips, Eindhoven, Netherlands) at 15 Kev, tilt angles between 6 and 12 degrees and variable magnifications up to 15,000×. Calibrated images were analyzed with MetaMorph software v.7.8 (Molecular Devices).

Transmission Electron Microscopy

Cellular and decellularized lung samples were cut into 2 mm cubes and stained with aqueous 1% osmium tetroxide (Electron Microscopy Sciences, Hatfield, PA) at room temperature for 2 hr. Samples were dried with a progressive ethanol gradient, and embedded in Araldite epoxy resin according to manufacturer procedure (RT13900 Kit; Electron Microscopy Sciences). After hardening, samples were cut with a diamond knife blade at 700 Å for ultrathin and 90 nm for semithin sections. Ultrathin sections were imaged with a Jeol JEM 1400 transmission electron microscope (JEOL Ltd., Tokyo, Japan), and semithin sections were stained with azure blue for light microscopy.

Statistical Analysis

The statistical analysis was based on measurements in at least three different rats. The unpaired Student's t test for samples of unequal variances was used to calculate statistical significance. The data was expressed as mean ± one standard deviation. The significance level for the sample distribution was defined as $P < 0.01$. The cumulative distribution function (CDF) was calculated to provide an estimate of interaction occurrences. The calculations were performed by XLStat (Addinsoft, Paris, France).

RESULTS

Spheres

The saccular stage of postnatal rat lung development, occurring between birth and postnatal day 4 (P4), is histologically characterized by large airspaces and thick primary septa (Fig. 1A). The saccular stage rapidly transitions into the alveolar stage. Largely complete by postnatal day 21 (P21) (Tschanz et al., 2014), the alveolar stage is characterized by septal thinning and the development of secondary septa that form the walls of new alveoli (Fig. 1B). Coincident with the development of secondary septa, the elastin cable line element can be detected at the tip of the secondary septa (Fig. 1C,D).

To investigate the morphologic events contributing to the development of the cable line element, we used a recently developed optical clearing method to examine the intact lung. Sca*l*e is an aqueous reagent the renders the lung optically transparent, but preserves intrinsic autofluorescence in the clarified lung (Hama et al., 2011). Unexpectedly, epifluorescence illumination of the Sca*l*ed postnatal lung specimens demonstrated a few autofluorescent spheres on P2 and innumerable spheres on P4 (Fig. 2A). To determine if the spheres represented cell-related artifact of the clearing method, we decelluarized the postnatal lungs and prepared PCLS (Fig. 2A). The lung slices were electrokinetically stained with eosin and examined by epi-illumination fluorescence microscopy. Again, we observed a peak of spheres on P4 with a rapid decline thereafter (Fig. 2B). High resolution light microscopy suggested a median sphere diameter of 1–2 μm (Fig. 2C).

Tropoelastin

To investigate the chemical properties of the spheres, a variety of histologic stains were used. Chemical staining generally produced little contrast; a notable exception was azur blue (Fig. 3A,B). TEM demonstrated spheres, but the average diameter was slighted smaller likely related to TEM sampling (Fig. 3C). SEM of both cellular and decellularized specimens demonstrated the broad spatial distribution of spheres within the primary septa (Fig. 3D). The green autofluorescence, selective fluorescence with eosin staining (Goldstein, 1969), and the size of the spheres suggested that these spheres

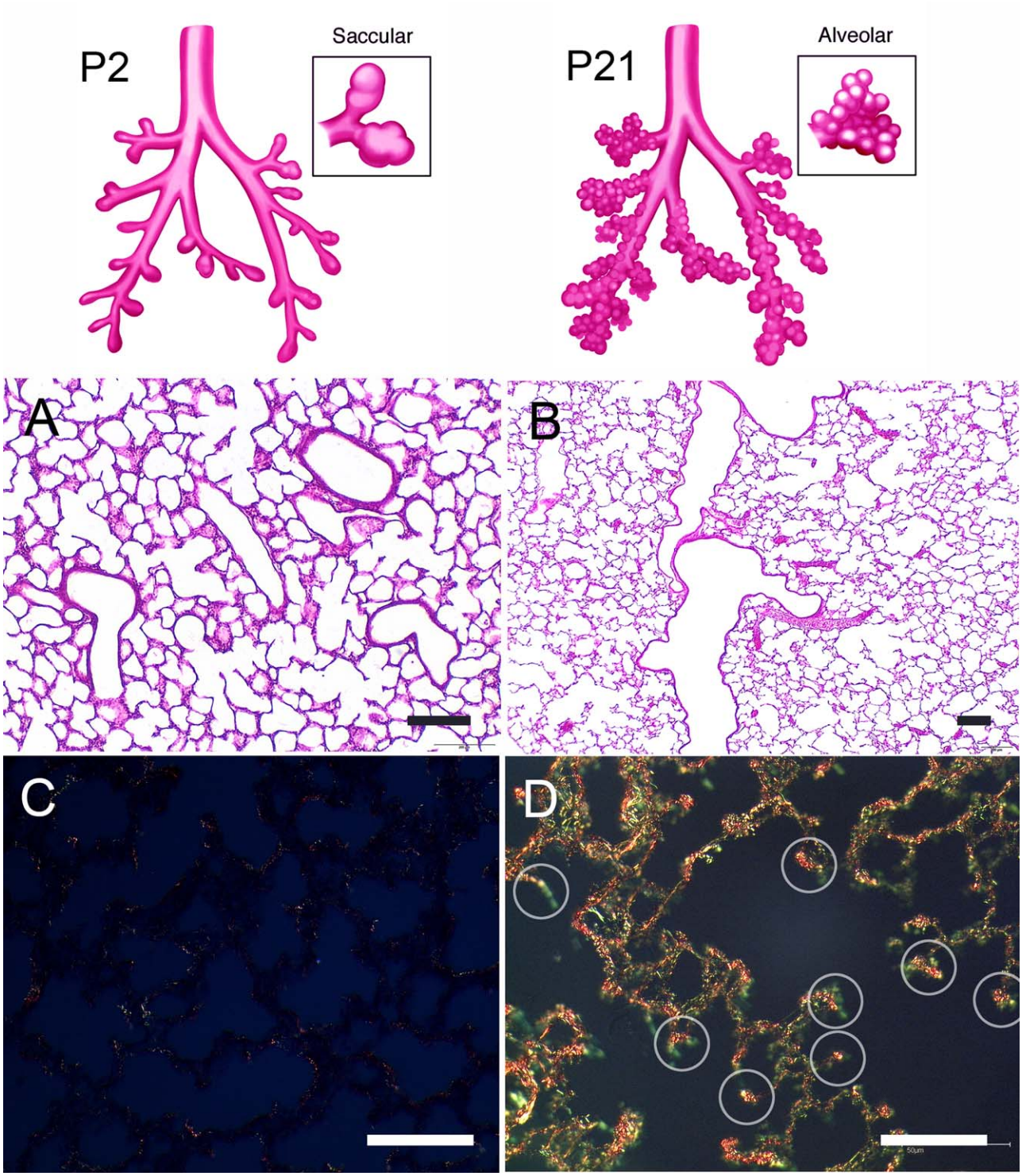

Fig. 1. The saccular and alveolar stages of rat lung development. (**A**) On postnatal day 2 (P2), the saccular stage is characterized by large airspaces and thickened septa. (**C**) Sirius red staining and fluorescence microscopy of decellularized lung at the end of the saccular stage (P4) demonstrated lttle evidence of collagen (yellow) or elastin (green) staining. (**B, D**) By the end of the alveolar stage (P21), the decellularized lung is characterized by secondary septations notable for collagen and elastin at the septal tips (circles). Bars = 100μm.

were tropoelastin (Mithieux et al., 2004). Since tropoelastin, the soluble form of elastin, is characterized by surface lysine residues, lung slices obtained from P4 rats were labeled with CFSE. Consistent with available lysine residues on the sphere surface, prominent staining of the P4 spheres was obtained with CFSE (Fig. 3E).

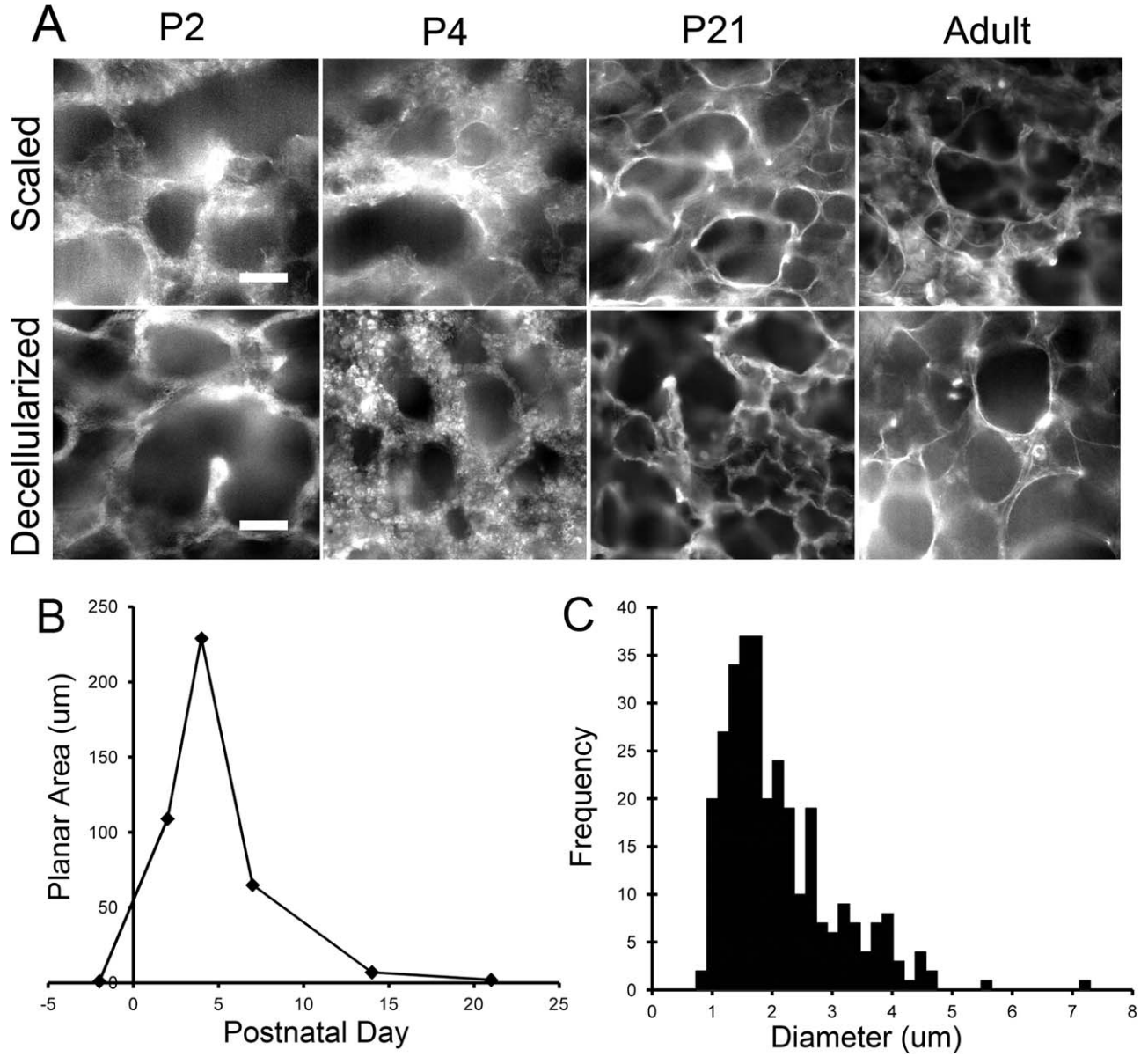

Fig. 2. Green autofluorescent spheres in the postnatal lung. (**A**) Sca*l*e reagent was used to render the intact lung optically transparent while retaining intrinsic autofluorescence. Epi-illumination fluorescence microscopy of the lung demonstrated innummerable autofluorescent spheres within the pimary septa. To exclude cell-related artifact, PCLS (500 μm) were prepared from decellularized postnatal lungs. Bar = 50 um. (**B**) In both preparations, the numbers of spheres peaked on P4 and were rarely detected by P21 (N = 10 rats). (**C**) Using high-resolution microscopy, the median diameter of the spheres was 1–2 μm.

Finally, staining of P4 lung slices with monoclonal anti-elastin antibody demonstrated specific labeling of the spheres (Fig. 3F).

Sphere-to-Cable Transition

To determine the temporal relationship between the appearance of the spheres and the subsequent development of the elastin cable line element, image stacks containing optical sections were obtained through representative lung slices on P4 and P14. Image analysis demonstrated numerous spheres uniformly distributed in the primary septa (Fig. 4A,C). By P14, there were few, if any, tropoelastin spheres but prominent staining of cable line element (Fig. 4B,D). The spatial relationship of the tropoelastin spheres and cells within the primary septa was investigated using TEM (Fig. 5). More than half of the spheres were unassociated with neighboring cells. No reproducible association of the spheres with myofibroblasts or other elastin-producing cells was observed.

Nascent Line Element and Scaffold Proteins

To define the extracellular interactions leading to formation of the cable line element, we decellularized

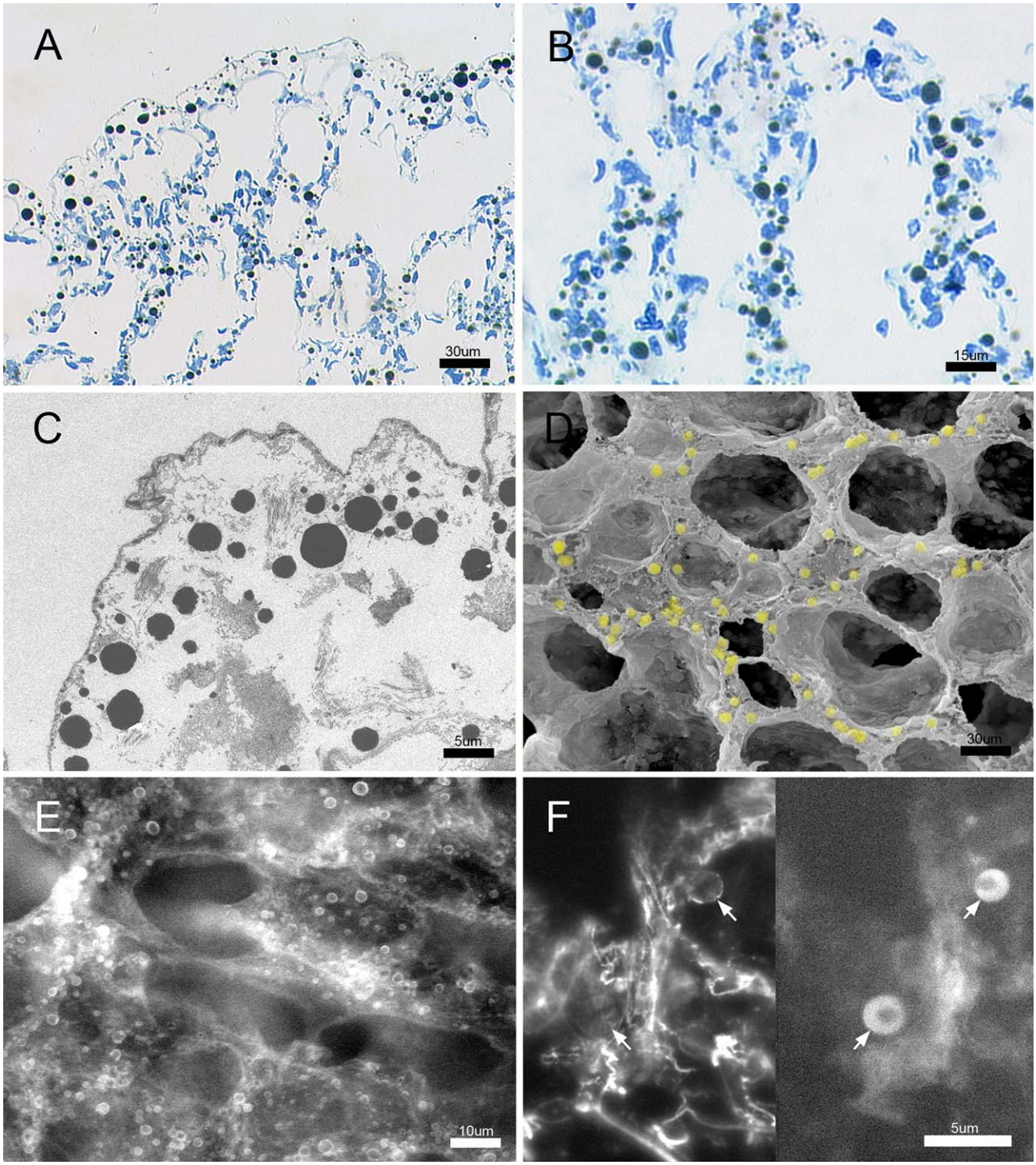

Fig. 3. Morphology and chemical identity of the spheres. (**A, B**) Azure blue staining provided sufficient contrast to demonstrate the broad distribution of the spheres on P4. (**C**) The spheres were electron dense by TEM. (**D**) SEM demonstrated that the spheres were located within the primary septa (P4 shown; yellow pseudocoloring for presentation purposes). (**E**) The presence of primary amines (lysine) on the surface of the spheres was confirmed by bright fluorescence staining after treatment with CFSE. (**F**) The identity of the spheres was confirmed by anti-tropoelastin monoclonal antibody.

postnatal lungs on P1, P2, P4, P7, P21, and adults. The spheres were uniformly distributed on P4, but demonstrated enhanced linearity by P7, and were absent in adults (Fig. 2B). Close examination of the linear spheres demonstrated apparent crosslinking of the tropoelastin spheres and associated scaffold proteins (Fig. 6). The

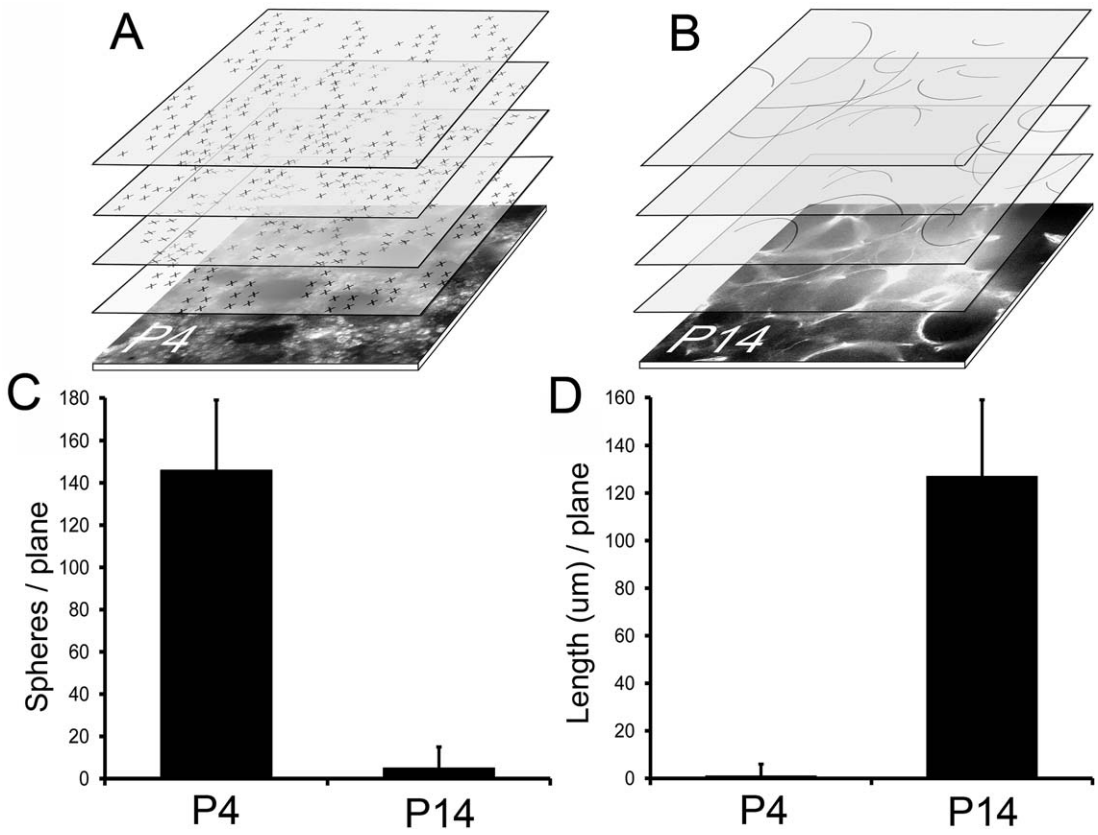

Fig. 4. Optical sections of tropoelastin spheres and the elastin cable line element. (**A, B**) PCLS on P4 and P14 were optically cleared with the Sca*l*e method and imaged with epi-illumination fluorescence microscopy. Optical sections were obtained at 50 μm intervals using modified structural illumination (Lee et al., 2009) and evaluated for the presence of spheres and cable line element. The schematic shows actual digital recombinations of image stacks on P4 and P14. (**C**) Spheres were densely and uniformly distributed throughout the image stack on P4, but rarely detected on P14. (**D**) In contrast, the cable line element was undetectable on P4, but prominent on P14.

attachment of the scaffold proteins to the tropoelastin spheres was frequently associated with apparent avulsions of portions of the spheres (Figs. 5 and 6, arrows). Already by P4, most spheres demonstrated multiple fiber contacts apparent by planar TEM projection (Fig. 6F). The spatial association of linearized tropoelastin and fiber-bound mature (insoluble) elastin (Fig. 5; asterisks) indicated that the tropoelastin spheres were an important intermediate in the development of the cable line element.

DISCUSSION

In this report, we defined the early morphologic development of the elastin cable line element in the postnatal rat lung. First, elastin in the postnatal rats was initially detected as 1–6 μm tropoelastin spheres; sphere concentration peaked on P4 and was largely absent by P14. Second, the tropoelastin spheres were uniformly distributed within the primary septa and randomly associated with parenchymal cells. Third, the linear assembly of the cable appeared to be dependent on crosslinking of the tropoelastin spheres to both collagen fibers and fibrillin microfibrils within the primary septa. We conclude that the rapid development of the elastin cable line element in the rat lung is facilitated by numerous tropoelastin spheres within the primary septa. The spatial organization of the cable line element appears to be independent of elastin deposition, but dependent on crosslinking to scaffold proteins within the primary septa.

A corollary of this observation is that the extracellular assembly of the cable line element—a structure responsible for maintaining gas exchange surface area, balancing alveolar surface forces and maintaining lung structure during ventilation—is a process responsive to mechanical forces. Previous work demonstrating the responsiveness of scaffold proteins to mechanical force distribution is consistent with this possibility. Tomoda et al. have studied the human lung and found that collagen fiber orientation closely relates to respiratory movement (Tomoda et al., 2013). Similarly, the axial orientation of collagen fibers can be achieved by mechanical loading of uncrosslinked fibers (Pins et al., 1997; Chow et al., 2014). Although less well-studied than collagen, fibrillin microfibrils subjected to stretch undergo gross changes in molecular conformation (Wang et al., 2009). Given that the cable line element extends from the central airways to the pleura (Wagner et al., 2015), the responsiveness of scaffold proteins to mechanical loading may also provide an explanation for the efficient development of the cable line element over organ-sized length scales.

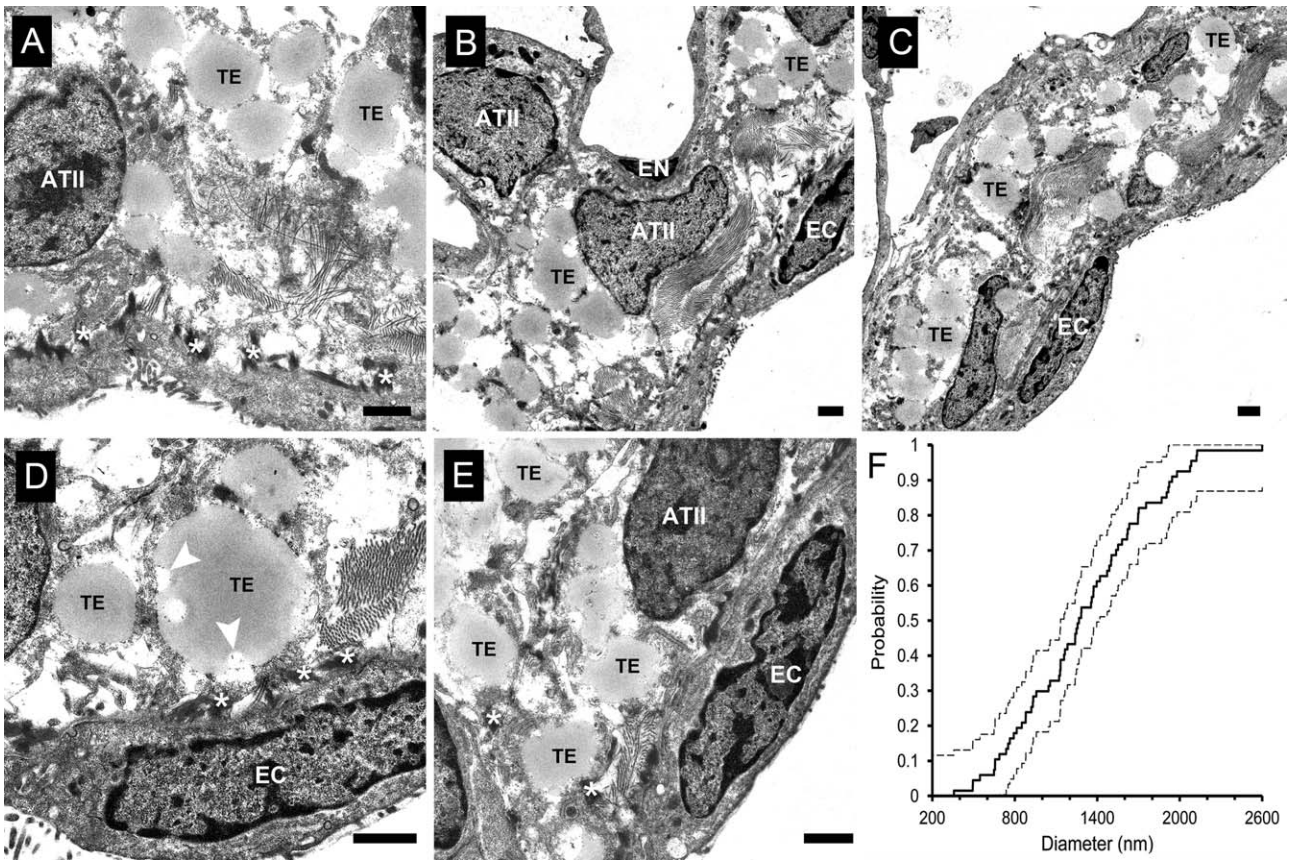

Fig. 5. Spatial relationship of tropoelastin spheres and cells within the primary septa. (**A–E**) The influence of cells within the primary septa on the distribution of tropoelastin spheres, the P1, P4, and P21 rat cellular lungs was studied by TEM. No consistent spatial relationship between spheres and cells was found; 56% of the spheres had no detectable cell contact by TEM. Surface avulsions were seen on P4 (D, arrows). Mature elastin (A, D; asterisks) was seen neighboring the avulsions. (**F**) As expected with a random spatial relationship, the probably of cell contact increased predictably with sphere diameter (95% confidence bands). 150 images were studied in N = 3 postnatal rats. TE, tropoelastin; ATII, alveolar type II cell; EC, epithelial cell; EN, endothelial cell. Bars = 1 um.

Tropoelastin, the soluble precursor of elastin, is secreted from cells as a 66–77 kDa protein in rats (Franzblau et al., 1989). The tropoelastin monomer has alternating hydrophobic and hydrophilic domains (Indik et al., 1987) that facilitate the self-assembly of tropoelastin—a process called coacervation—into quantized spheres (Wise and Weiss, 2009). Lysine residues on the sphere surface facilitate the enzyme-dependent cross-linking of tropoelastin spheres not only to other spheres, but also to extracellular scaffold proteins (Kagan and Trackman, 1991). Our findings provide *in vivo* support for the view that tropoelastin coacervation is an adaptive process that facilitates the efficient delivery of chemically available tropoelastin (Clarke et al., 2006). In our TEM studies, we found no evidence that cells, such as myofibroblasts, localized the deposition or alignment of soluble elastin. In contrast, the diffuse "blanket" of tropoelastin spheres on P4 further indicates that tropoelastin production is not spatially directed. Rather, the linear alignment of the P14 elastin cable line element appears to be dependent on extracellular fiber interactions.

There are numerous extracellular components potentially contributing to the assembly of the elastin cable line element. Nearly 40 different molecules, identified by microscopy and immunohistochemical approaches, have been found to interact with elastic fibers and fibrillin microfibrils (Baldwin et al., 2013). The numerous interacting molecules complicate attempts to evaluate the function of individual molecules by selective gene manipulation *in vivo*. Similarly, the three-dimensional structure of the cable line element and the dynamic mechanical milieu of the lung complicate manipulations *in vitro*. Here, we used a variety of imaging approaches to demonstrate the extracellular assembly of the cable line element. In particular, our TEM images emphasized the importance of collagen fibers and fibrillin microfibrils in cable assembly.

The spatial alignment of the line element, with little evidence indicating cellular instruction, suggests that cable alignment is not determined by a specific genetic program, but rather self-organized by physicochemical interactions within the extracellular matrix. These *in vivo* observations are reminiscent of *in vitro* observations of elastin self-assembly (Keeley et al., 2002; Tu et al., 2010). We anticipate that lung ventilation provides not only an energy source for this process, but also a stretch field capable of informing the adaptive development of its structure. Clinically, the possibility of self-organized

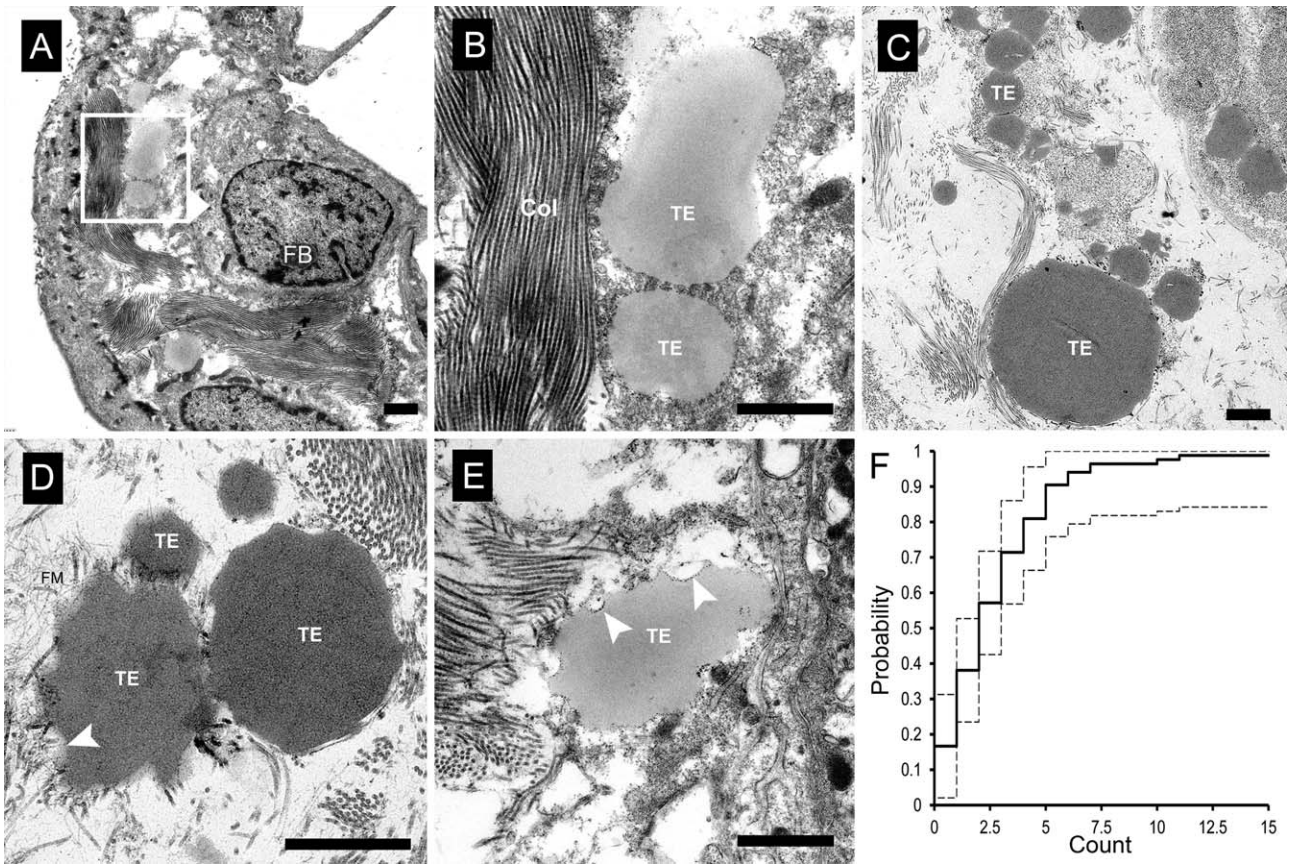

Fig. 6. Fiber interactions with tropoelastin spheres. (**A–E**) TEM demonstrated prominent extracellular fiber interactions with the tropoelastin spheres in cellular (A, B, E) and decellularized (C, D) lungs. Electron-dense attachments of fibers with characteristic collagen banding and the beaded appearance of fibrillin microfibrils were frequently associated with the surface of the tropoelastin spheres. In regions of dense sphere-fiber interactions, readily identifiable areas of apparent surface avulsion (arrows) were common. The potential influence of the extracellular fibers on the linear alignment of tropoelastin was apparent in both subpleural and septal TEM images. (**F**) The cumulative distribution function reflects the number of fiber interactions detected per sphere (95% confidence band); 440 TEM images in N = 12 rats. TE, tropoelastin; Col, collagen; FM, fibrillin microfibrils; FB, fibroblast. Bars = 1 um.

development of the cable line element provides a new focus for studies of bronchopulmonary dysplasia and ventilator-induced lung injury.

ACKNOWLEDGEMENTS

The authors would like to thank Dr. Anthony Weiss, Dr. Robert Mecham and Dr. Christoph Brockhausen for helpful discussions. The authors also thank Charlotte A. J. Hutchinson for her translation of Dubreuil, et al.

LITERATURE CITED

Azcuy A, Foraker AG, Anderson AE. 1962. Morphological spectrum of aging and emphysematous lungs. Ann Intern Med 57:1–17.

Baldwin AK, Simpson A, Steer R, Cain SA, Kielty CM. 2013. Elastic fibres in health and disease. Expert Rev Mol Med 15:e8.

Burri PH, Dbaly J, Weibel ER. 1974. Postnatal-growth of rat lung. 1. Morphometry. Anat Rec 178:711–730.

Butler JP, Oldmixon EH, Hoppin FG. 1996. Dihedral angles of septal "bend" structures in lung parenchyma. J Appl Physiol 81: 1800–1806.

Carey MA, Card JW, Voltz JW, Arbes SJ, Germolec DR, Korach KS, Zeldin DC. 2007. It's all about sex: Gender, lung development and lung disease. Trends Endocrinol Metab 18:308–313.

Chow MJ, Turcotte R, Lin CP, Zhang YH. 2014. Arterial extracellular matrix: A mechanobiological study of the contributions and interactions of elastin and collagen. Biophys J 106:2684–2692.

Clarke AW, Arnspang EC, Mithieux SM, Korkmaz E, Braet F, Weiss AS. 2006. Tropoelastin massively associates during coacervation to form quantized protein spheres. Biochemistry 45:9989–9996.

Dubreuil G, Lacoste A, Raymond R. 1936. Observations sur le developpement du poumon humain. Bull Histol Appl Tech Microsc 13:235–245.

Franzblau C, Pratt CA, Faris B, Colannino NM, Offner GD, Mogayzel PJ, Troxler RF. 1989. Role of tropoelastin fragmentation in elastogenesis in rat smooth-muscle cells. J Biol Chem 264: 15115–15119.

Goldstein DJ. 1969. The fluorescence of elastic fibers stained with eosin and excited by visible light human animal. Histochem J 1: 187–198.

Hadchouel A, Franco-Montoya ML, Delacourt C. 2014. Altered lung development in bronchopulmonary dysplasia. Birth Defects Res A 100:158–167.

Haidar A, Ryder TA, Wigglesworth JS. 1991. Failure of elastin development in hypoplastic lungs associated with oligohydramnios – An electron-microscopic study. Histopathology 18: 471–473.

Hama H, Kurokawa H, Kawano H, Ando R, Shimogori T, Noda H, Fukami K, Sakaue-Sawano A, Miyawaki A. 2011. Scale: a chemical approach for fluorescence imaging and reconstruction of transparent mouse brain. Nat Neurosci 14:1481–1488.

Harding R, Hooper SB, Han VKM. 1993. Abolition of fetal breathing movements by spinal-cord transection leads to reductions in fetal lung liquid volume, lung growth, and IFG-II gene-expression. Pediatr Res 34:148–153.

Heo YS, Song HJ. 2011. Characterizing cutaneous elastic fibers by eosin fluorescence detected by fluorescence microscopy. Ann Dermatol 23:44–52.

Indik Z, Yoon K, Morrow SD, Cicila G, Rosenbloom J, Rosenbloom J, Ornsteingoldstein N. 1987. Structure of the 3′ region of the human elastin gene - Great abundance of alu repetitive sequences and few coding sequences. Connect Tissue Res 16:197–211.

Jensen T, Roszell B, Zang F, Girard E, Matson A, Thrall R, Jaworski DM, Hatton C, Weiss DJ, Finck C. 2012. A rapid lung de-cellularization protocol supports embryonic stem cell differentiation in vitro and following implantation. Tissue Eng Pt C-Meth 18:632–646.

Kagan HM, Trackman PC. 1991. Properties and function of lysyl oxidase. Am J Respir Cell Mol Biol 5:206–210.

Keeley FW, Bellingham CM, Woodhouse KA. 2002. Elastin as a self-organizing biomaterial: Use of recombinantly expressed human elastin polypeptides as a model for investigations of structure and self-assembly of elastin. Philos T Roy Soc B 357:185–189.

Lee GS, Miele LF, Turhan A, Lin M, Hanidziar D, Konerding MA, Mentzer SJ. 2009. Spatial calibration of structured illumination fluorescence microscopy using capillary tissue phantoms. Microsc Res Tech 72:85–92.

Lindahl P, Karlsson L, Hellstrom M, GebreMedhin S, Willetts K, Heath JK, Betsholtz C. 1997. Alveogenesis failure in PDGF-A-deficient mice is coupled to lack of distal spreading of alveolar smooth muscle cell progenitors during lung development. Development 124:3943–3953.

Mithieux SM, Rasko JEJ, Weiss AS. 2004. Synthetic elastin hydrogels derived from massive elastic assemblies of self-organized human protein monomers. Biomaterials 25:4921–4927.

Pierce RA, Albertine KH, Starcher BC, Bohnsack JF, Carlton DP, Bland RD. 1997. Chronic lung injury in preterm lambs: Disordered pulmonary elastin deposition. Am J Physiol-Lung C 272: L452–L460.

Pins GD, Christiansen DL, Patel R, Silver FH. 1997. Self-assembly of collagen fibers. Influence of fibrillar alignment and decorin on mechanical properties. Biophys J 73:2164–2172.

Puchtler H, Waldrop FS, Valentin L. 1973. Polarization microscopic studies of connective-tissue stained with picro-sirius red FBA. Beitrage Pathol 150:174–187.

Schittny JC, Burri PH. 2008. Development and growth of the lung. In: Fishman AP, Elias JA, Fishman JA, Grippi MA, Senior RM, Pack AI, editors. Fishman's pulmonary diseases and disorders, 4th ed. McGraw-Hill, New York. p 91–114.

Sweat F, Rosentha.Si, Puchtler H. 1964. Sirius red F3BA as stain for connective tissue. Arch Pathol 78:69–72.

Thurlbeck WM, Kida K, Langston C, Cowan MJ, Kitterman JA, Tooley W, Bryan H. 1979. Postnatal lung growth after repair of diaphragmatic-hernia. Thorax 34:338–343.

Tomoda K, Kimura H, Osaki S. 2013. Distribution of collagen fiber orientation in the human lung. Anat Rec 296:846–850.

Tschanz SA, Salm LA, Roth-Kleiner M, Barre SF, Burri PH, Schittny JC. 2014. Rat lungs show a biphasic formation of new alveoli during postnatal development. J Appl Physiol 117:89–95.

Tu YD, Wise SG, Weiss AS. 2010. Stages in tropoelastin coalescence during synthetic elastin hydrogel formation. Micron 41:268–272.

Wagner W, Bennett RD, Ackermann M, Ysasi AB, Belle JM, Valenzuela CD, Pabst AM, Tsuda A, Konerding MA, Mentzer SJ. 2015. Elastin cables define the axial connective tissue system in the murine lung. Anat Rec 298:1960–1968.

Wang MC, Lu YH, Baldock C. 2009. Fibrillin microfibrils: A key role for the interbead region in elasticity. J Mol Biol 388:168–179.

Weibel ER. 1986. Functional morphology of lung parenchyma. In: Macklem PT, Mead J, editors. Mechanics of Breathing, part 1, Handbook of physiology, sec 3: The Respiratory System. Bethesda, Md., American Physiological Society. vol 3, p 89–111.

Weibel ER. 2012. Commentaries on viewpoint: Unresolved mysteries change. Perspect J Appl Physiol 113:1948–1948.

Wendel DP, Taylor DG, Albertine KH, Keating MT, Li DY. 2000. Impaired distal airway development in mice lacking elastin. Am J Respir Cell Mol Biol 23:320–326.

Wilson TA, Bachofen H. 1982. A model for mechanical structure of the alveolar duct. J Appl Physiol 52:1064–1070.

Wise SG, Weiss AS. 2009. Tropoelastin. Int J Biochem Cell Biol 41: 494–497.